International Journal of Applied Earth Observations and Geoinformation 110 (2022) 102806

Contents lists available at ScienceDirect

International Journal of Applied Earth Observations and Geoinformation

journal homepage: www.elsevier.com/locate/jag

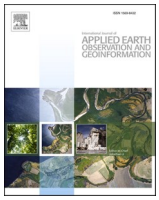

Demystifying LandTrendr and CCDC temporal segmentation

Valerie J. Pasquarella [a,b,*], Paulo Arévalo [a], Kelsee H. Bratley [a], Eric L. Bullock [c], Noel Gorelick [d,e], Zhiqiang Yang [c], Robert E. Kennedy [f]

[a] Department of Earth and Environment, Boston University, Boston, MA 02215, USA
[b] Harvard Forest, Harvard University, Petersham, MA 01366, USA
[c] USFS Forest Service Rocky Mountain Research Station, Ogden, UT 84401, USA
[d] Google Switzerland, Zurich 8002, Switzerland
[e] Remote Sensing Laboratories, University of Zürich, Zürich 8057, Switzerland
[f] College of Earth, Ocean, and Atmospheric Sciences, Oregon State University, Corvallis, OR 97331, USA

ARTICLE INFO

Keywords:
Time series
Temporal segmentation
Change detection
LandTrendr
CCDC
Google Earth Engine

ABSTRACT

Improved access to remotely sensed imagery and time series algorithms in combination with increased availability of cloud computing resources and platforms such as Google Earth Engine have significantly expanded the community of users processing and analyzing time series of satellite observations. Though individual time series analysis methods and their applications tend to be well-documented, comparisons of different approaches are beneficial to new users faced with the choice of different algorithms and parameterizations. We review two temporal segmentation approaches that have become increasingly prevalent in land cover mapping and monitoring: LandTrendr (Landsat-based detection of Trends in Disturbance and Recovery) and CCDC (Continuous Change Detection and Classification). We examine differences in the way these approaches use the temporal and spectral domains and compare model specifications and outputs. This review highlights previous work and applications, current limitations, ongoing challenges, and opportunities for future integration and comparison of methods and map products, and is expected to benefit both user and developer communities.

1. Introduction

With unprecedented access to satellite imagery and cloud-based processing capabilities, more users are working with multi-temporal Earth observation datasets than ever before (Gorelick et al., 2017; Wulder et al., 2012). Following the opening of the Landsat archive in 2008, time series-based approaches for land cover mapping and change detection have become increasingly common and remain an active area of development, both in terms of methods and theory (Banskota et al., 2014; Chaves et al., 2020; Gómez et al., 2016; Hemati et al., 2021; Woodcock et al., 2020). Though more granular taxonomies for characterizing change detection approaches have been proposed (e.g., Zhu, 2017), we consider the broad class of temporal segmentation algorithms to include methods that group observations into larger representative periods of time or "segments" such that a single model is applied within a segment and different models are applied across segments. These piecewise fitting approaches can be viewed as a temporal equivalent to spatial segmentation algorithms, which use spectral properties to group contiguous pixels into shapes representing larger landscape objects or patches (e.g., Hossain and Chen, 2019). Characterization of temporal segments enables analysis of both short- and long-term trends and patterns in landscape properties and surface conditions. However, the types of change processes and events that can be identified are intrinsically linked to the algorithm used to perform temporal segmentation (Kennedy et al., 2014).

Two temporal segmentation approaches that are becoming more prevalent in natural resource monitoring applications are the LandTrendr (Landsat-based detection of Trends in Disturbance and Recovery) and CCDC (Continuous Change Detection and Classification) algorithms (Zhu, 2017). Though the use of these approaches was once limited to a small subset of users with sufficient data storage and processing capabilities, both LandTrendr (Kennedy et al., 2010) and CCDC (Zhu et al., 2012; Zhu and Woodcock, 2014) have since been implemented in Google Earth Engine (Arévalo et al., 2020a; Kennedy et al., 2018b). Implementation in Earth Engine's cloud computing environment has enabled a global community of users to run these and other temporal segmentation methods, such as Exponentially Weighted Moving Average Change Detection (EWMACD; Brooks et al., 2014), Vegetation

* Corresponding author at: Department of Earth and Environment, Boston University, Boston, MA 02215, USA.
E-mail address: valpasq@bu.edu (V.J. Pasquarella).

https://doi.org/10.1016/j.jag.2022.102806
Received 29 January 2022; Received in revised form 11 April 2022; Accepted 29 April 2022
Available online 13 May 2022

Change Tracker (VCT; Huang et al., 2010) and Vegetation Regeneration and Disturbance Estimates through Time (VeRDET; Hughes et al., 2017). Furthermore, both LandTrendr and CCDC are being used operationally for large-area mapping and monitoring efforts (e.g., Brown et al., 2019; Kennedy et al., 2018a; Lister et al., 2020; Tarrio et al., 2019; Xian et al., 2021; Zhu et al., 2016). Therefore, we anticipate continued increases in the use of these algorithms as well as their derivative products.

With a growing user community, it is increasingly important to build a comprehensive understanding of the assumptions, advantages, and limitations of individual algorithms as well as differences across approaches (Zhu, 2017). In the case of LandTrendr and CCDC, both algorithms partition time series of observations into sequences of modeled temporal segments, both can be used to produce annual land cover and land cover change map products, and both can generate smoothed or "synthetic" imagery. However, these algorithms fundamentally differ in their segmentation approaches, interpretation of the resulting model fits, and output datasets. Quantitative assessments using independent reference data for specific change detection applications have been addressed in other studies such as Cohen et al. (2017), who present a more comprehensive comparison of forest disturbance maps generated using different temporal segmentation approaches. In this paper, we use cases from previously published studies as well as illustrative, single-pixel examples to review key decisions in working with the LandTrendr and CCDC algorithms. This focused, in-depth perspective is intended to aid users in interpreting results and products and serve as an inroad for further comparisons with other temporal segmentation approaches.

2. Overview of algorithms

The LandTrendr and CCDC algorithms are both well-documented in previous publications (see Kennedy et al., 2012, 2010; Saxena et al., 2018; Zhu and Woodcock, 2014), and code is available in open-source repositories (e.g., Table 1**)**. Our objective here is not to revisit the mechanics of these mature and widely cited temporal segmentation algorithms, but to review fundamental design choices and sensitivities to user-specified inputs. Specifically, we consider how LandTrendr and CCDC use the temporal domain for segmentation (*Section 2.1)*, the influence of temporal and spectral inputs on model fitting (*Sections 2.2 and 2.3*), and additional considerations in selecting parameter inputs (*Section 2.4*). We also summarize key model outputs and derived data products (*Section 2.5*) and related visualization tools (*Section 2.6*).

Table 1
Examples of LandTrendr and CCDC implementations.

Algorithm implementation	Key publications	Links to code
Original LandTrendr implementation	Kennedy et al., 2010	https://github.com/KennedyResearch/LandTrendr-2012
LandTrendr in Google Earth Engine	Kennedy et al., 2018b	https://github.com/eMapR/LT-GEE
USGS LCMAP PyCCD	Zhu et al., 2016 Brown et al., 2019 Xian et al., 2021	https://code.usgs.gov/lcmap/pyccd
Global Environmental Remote Sensing Laboratory (GERSL) CCDC	Zhu et al., 2012 (v1.0) Zhu and Woodcock, 2014 (v7.3)	https://github.com/GERSL/CCDC (v12.3)
GERSL COLD (COntinuous monitoring of Land Disturbance)	Zhu et al., 2020	https://github.com/GERSL/COLD

2.1. Use of the temporal domain

Landscape change processes occur at many time scales and may include intra-annual (seasonal) changes in phenology and condition, as well as inter-annual processes such as abrupt shifts in land cover, long-term trends, and more complex disturbance-recovery trajectories (Coppin et al., 2004; Pasquarella et al., 2016; Vogelmann et al., 2016). The frequency of observations used to detect and model temporal dynamics directly influences the types of processes that can be characterized using time series of remotely sensed observations (Kennedy et al., 2014). Though temporal segmentation methods can be generalized to any time series of continuous values, LandTrendr and CCDC were both originally developed to take advantage of the unparalleled temporal coverage of the Landsat record and both algorithms typically use full Landsat collections as inputs. However, there are notable differences in how they reduce and analyze an observation record for a given pixel.

The LandTrendr approach is typically applied to time series data where one observation or value is selected to represent each year. Standard use of medoid composites is intended to minimize the influence of vegetation phenology, effectively controlling for seasonal variability prior to modeling temporal trajectories, and spectral values from different Landsat sensors are harmonized using transformations proposed by Roy et al. (2016). LandTrendr segmentation interprets input time series as continuous piecewise trajectories, which are typically described in terms of "segments" and "vertices" (Fig. 1). Because LandTrendr segmentation is performed on time series with an annual time step, change processes are associated with a year of detection rather than a specific date (month/day) of change.

In contrast, CCDC segmentation is typically performed using a time series of all clear observations. This approach attempts to detect change at the native frequency of the input time series such that changes can be associated with a particular acquisition date rather than a composite year. To explicitly account for intra-annual cyclic patterns in surface reflectance signals resulting from changes in illumination conditions, atmospheric conditions, and vegetation phenology, CCDC uses linear harmonic models that include sine and cosine terms. These harmonic terms eliminate the need to pre-specify a compositing period and provide a larger set of coefficients/features that can be used for segment-based classification (e.g., Pasquarella et al., 2018; Zhu et al., 2016; Zhu and Woodcock, 2014). Unlike LandTrendr fitting, where vertices represent shared segment start/end dates, CCDC fits input time series using a discontinuous piecewise model consisting of independent segments and "breaks," where breaks correspond to discrete change events represented as jumps or offsets in the temporal trajectory (Fig. 1). In some cases, harmonic model fitting may be unstable because of the small numbers of observations used in fitting, leading to extended gap periods between CCDC model segments (Fig. 2). Forward- or back-filling of CCDC parameters from adjacent segments or use of a "disturbed" category in segment-based classification can be applied to reconcile these gap periods. In comparison, LandTrendr will always produce a continuous trajectory.

Because both algorithms assume a simple linear relationship between time and reflectance (or other modeled value), they are well-suited for identifying periods of stability or relatively stable rates of change, and segments can be characterized in terms of direction of change (stable, loss or gain) and sorted in terms of change magnitude and duration. However, nonlinear dynamics, that is, periods with increasing, decreasing, or otherwise nonstationary rates of change, are more challenging to approximate using linear basis functions (Fig. 2). Thus, in addition to discrete events, such as abrupt disturbances and changes in land cover, breaks and vertices may more generally represent approximate points of inflection in the rate of the fitted trajectory.

2.2. Temporal considerations

Ability to fit temporal trajectories and identify disturbances and

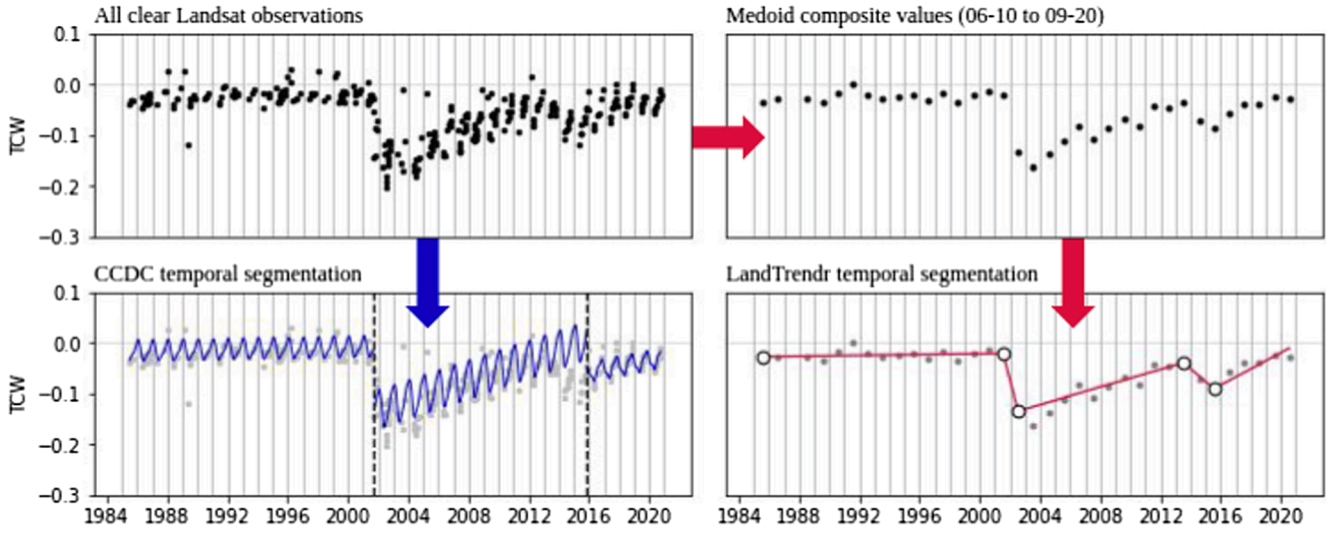

Fig. 1. Examples of CCDC and LandTrendr inputs and segmentation results for a site in Maine, USA (45.4189°, −69.8050°). This site was initially forested before undergoing disturbance events around 2002 and 2015–2016 that were each followed by periods of regrowth, as suggested by an increasing trend in Tasseled Cap Wetness (TCW). CCDC models were fit to all clear Landsat observations, resulting in two model breaks (dashed black lines) and three discrete segments characterized by different linear trends and seasonal harmonic amplitudes (solid blue lines). LandTrendr does not explicitly characterize seasonal variability, instead using seasonal compositing to control for phenological differences prior to segmentation. The LandTrendr segmentation result is based on medoid composites for June 10 to September 20 (Northern Hemisphere growing season), and includes five segments (solid red lines) and associated vertices (open black circles).

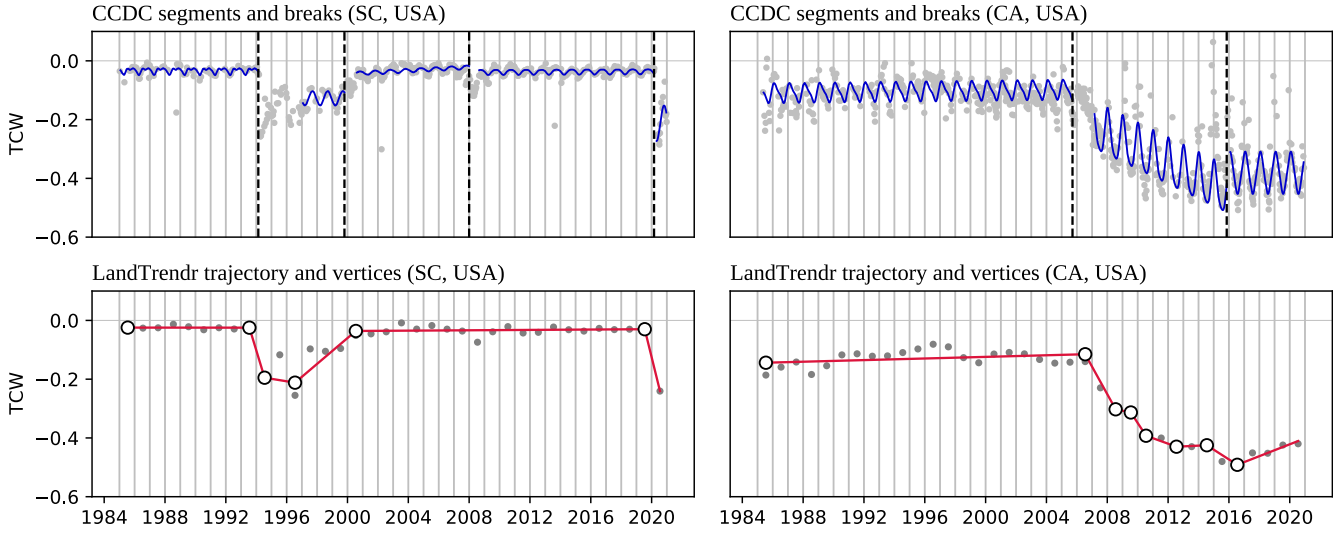

Fig. 2. Examples of CCDC segments and breaks and LandTrendr trajectory and vertices. Left: Tasseled Cap Wetness (TCW) segmentation for a plantation forest that has experienced multiple harvest/disturbance events, South Carolina, USA (33.3253°, −79.6437°). Right: TCW segmentation for an orchard in the Central Valley, California, USA (37.5298°, −120.9505°) that was cleared around 2007.

other change processes is largely determined by the number of clear observations available for analysis at both scene and pixel levels (Kennedy et al., 2014). Long-term satellite observation records like the Landsat archive vary both spatially and temporally because of clouds, shadows, snow/ice masking, scan line gaps, orbital path overlap, and image processing levels and archiving (Egorov et al., 2019; Wulder et al., 2016). Thus, when performing temporal segmentation, users should always consider ecosystems and/or processes of interest and site-specific patterns in observation frequency, including regularly occurring seasonal gaps (like those that occur in high latitudes because of low solar zenith angles) as well as periods of missing data corresponding to archival gaps, and adjust their choice of segmentation algorithm and algorithm-specific parameters accordingly.

Because LandTrendr segmentation relies on a single observation or value per year, appropriate selection of compositing period start and end dates is critical, and "best available pixel" composites for regions of interest at high latitudes are more likely to encounter issues related to phenology, whereas composites for locations closer to the equator are more likely to encounter issues related to persistent cloud cover (Banskota et al., 2014). Examples of compositing periods for previous studies using LandTrendr are provided in Table 2. Studies focused on Northern Hemisphere forest dynamics typically define the compositing period to approximate the growing season, with start dates in June or July and end dates in August or September (e.g., Frazier et al., 2015; Griffiths et al., 2012; Kennedy et al., 2010; Pflugmacher et al., 2012; Senf and Seidl, 2021). However, growing season start and end dates must be adjusted when considering vegetation dynamics in the Southern Hemisphere (e.g., Mugiraneza et al., 2020; Nguyen et al., 2018). The compositing period may also be set to characterize finer-grained local seasonality (e.g., De Marzo et al., 2021; Gelabert et al., 2021) or

Table 2
Examples of studies using LandTrendr temporal segmentation, including process of interest, study area, temporal compositing period and years analyzed, and spectral or other time series inputs used for segmentation.

Study	Process	Study area	Temporal period	Spectral inputs*
Kennedy et al., 2010	Forest disturbance	Pacific Northwest United States	Mid-July to late August 1985–2007	TCW, NBR, NDVI
Griffiths et al., 2012	Forest disturbance and recovery dynamics	Central-eastern Romania	Early June to mid-September 1984–2010	TCW
Pflugmacher et al., 2012	Disturbance history as a predictor of forest structural attributes	Blue Mountains of eastern Oregon	Mid-July and August 1972–2010	TCA
Main-Knorn et al., 2013	Biomass dynamics	Beskid Mountains, Northwestern Carpathian Mountain Range, Europe	29 June to 7 October (DOY 180–280), 1985–2010	Biomass predictions
Frazier et al., 2014	Temporal trajectory metrics as a predictor of forest attributes	Northeast British Columbia/southeast Yukon Territory, Canada	Closest to 19 July (Julian day 200) anniversary date, 1984–2012,	TCW
Frazier et al., 2015	Forest disturbance and recovery processes	Boreal Shield ecozone, Canada	June, July, and August, target 19 July (Julian day 200) anniversary date, 1985–2012	TCW
Grogan et al., 2015	Forest disturbance	Cambodian–Vietnamese border	Julian day 300 anniversary date, (±60 days for seasonal forest; beginning of May to end of April of the following year for evergreen forest), 1989–2013	NDVI, NBR, TCW, TCB, TCA
Meigs et al., 2015	Tree mortality due to mountain pine beetle and western spruce budworm outbreaks	Oregon and Washington, United States	Clearest pixel per year near the median date of each stack (generally August 1st), 1984–2012	NBR
Senf et al., 2015	Defoliator and bark beetle disturbances	British Columbia, Canada	±30 days around 15 July 1990–2013	NBR
Reilly et al., 2017	Fire extent and burn severity	Oregon and Washington, United States	Mid-July to late August 1985–2010	NBR
Schneibel et al., 2017	Cultivation patterns and deforestation dynamics	South-central Angola	May to June 1989–2013	NBR
Dara et al., 2018	Cropland abandonment and recultivation	Northern Kazakhstan and border areas of Russia	Annual time series, 1984–2016	Cropland probabilities
Kennedy et al., 2018a	Forest biomass monitoring	Western Cascades province of Oregon and a small part of California, United States	1 July to 31 August 1990–2012	NBR, TCW, SWIR1
Nguyen et al., 2018	Forest disturbance and recovery	Victoria, Australia	December to March (15 January anniversary date ± 45 days), 1987–2016	NBR
Yang et al., 2018	Disturbance and recovery in surface mining areas	Curragh Mine, Australia	April to July 1988–2015	NDVI
Yin et al., 2018	Agricultural land abandonment	Georgia and the North Caucasian Federal District of Russia	Annual time series, 1985–2015	Agricultural land probabilities
Bright et al., 2019	Post-fire vegetation recovery	Twelve named wildfire events in western North America that burned during the years 2000 to 2007	1 June to 30 September 1984–2016	NBR
Hislop et al., 2019	Forest disturbance	Victoria, Australia	First clear pixel closest to February 15, 1988–2017	NBR, NDVI, TCW
Shimizu et al., 2019b	Classification of disturbance agents	Bago Mountain Range, Myanmar	1 October to 31 January 1999–2018	TCB, TCG, TCW, TCA, NBR
D. Tang et al., 2019	Forest disturbance	China–Laos border	February and March (Julian day 60 anniversary date), 1988–2016	ARVI
Xu et al., 2019	Conversion from vegetation to impervious surface	City of Nanjing, Jiangsu Province, China	1 June to 30 September 1988–2018	NBR, NDVI, NDMI, Red, SWIR2
Zhu et al., 2019	Croplands conversion	Dongting Lake, China	June to September 1998–2018	NDVI
Mugiraneza et al., 2020	Land cover mapping	Kigali, Rwanda	1 September to 30 June of the following year, 1987–2019	Red, SWIR1, NDVI, NDMI, TCG, TCW
Rathnayake et al., 2020	Land use/land cover change	Sri Lanka	1 January to 31 December 1991–2018	NBR, NDVI
Vogeler et al., 2020	Forest disturbance characterization and change agent attribution	Minnesota, United States	1 July to 9 September 1972–2019	TCB, TCG, TCW, TCA
Xiao et al., 2020	Mining disturbances and land reclamation	Shengli Coalfield, Inner Mongolia	1 January to 30 December 2003–2019	NDVI
de Jong et al., 2021	Mangrove cover change	Suriname coast	1 January to 31 December (annual), 2000–2018	NDVI
De Marzo et al., 2021	Forest disturbance and degradation	Dry Chaco, Northern Argentina	May-July (dry season), February-April (pre-dry season) and August-October (post-dry season), 1987–2017	TCW, NBR, NDMI
Gelabert et al., 2021	Secondary succession and woody encroachment in semi-natural grasslands	Spanish side of the Pyrenees mountain range	March-May (spring), June-August, (summer) September- November (autumn), 1984–2019	TCB, TCG, TCW, TCA
Murillo-Sandoval et al., 2021	Land cover change	Andes-Amazon, Colombia	1988–2019	NBR
Rodman et al., 2021	Tree mortality due to wildfire and spruce beetle outbreaks	San Juan Mountains, Southwestern Colorado, United States	1 July to 30 September 1984–2019	NBR
Senf and Seidl, 2021	Forest disturbance	Continental Europe	1 June to 30 September, 1986–2016	SWIR1, SWIR2, TCW, NBR
Ye et al., 2021	Gradual forest change in red soil areas	Hengyang, Hunan Province, China	1 January to 31 December (annual), 1985–2019	DSVI

* Spectral Index abbreviations: ARVI = Atmospherically Resistant Vegetation Index, DSVI = Disturbance Sensitive Vegetation Index, NBR = Normalized Burn Ratio, NDFI = Normalized Difference Forest Index, NDMI = Normalized Difference Moisture Index, NDVI = Normalized Difference Vegetation Index, TCA = Tasseled Cap Angle, TCB = Tasseled Cap Brightness, TCG = Tasseled Cap Greenness, TCW = Tasseled Cap Wetness.

extended to create a true annual composite based on all observations from a given year (e.g., de Jong et al., 2021; Rathnayake et al., 2020; Xiao et al., 2020; Ye et al., 2021). Both the number of fitted LandTrendr segments and timing of vertices can vary depending on how the compositing period is specified (Fig. 3). Therefore, users are encouraged to experiment with composite start and end dates for example sites prior to performing segmentation at landscape scales. In some cases, users might also consider modifying the compositing method. For example, maximum spectral values might be more useful than medoid composites in agricultural settings or other ecosystems where seasonal cycles are less regular.

Although CCDC attempts to fit all available observations for a given pixel (Fig. 3), users must still consider how spatial and temporal variability in the frequency of observations may affect segmentation results. Examples of time periods used in previous studies employing the CCDC segmentation approach are shown in Table 3. Because CCDC identifies break points based on the consecutive number of observations that deviate from the predicted trajectory of the current segment, when there are long periods of missing data (e.g., full years with no observations), there will be a greater tendency to find breaks after these periods, resulting in an artificially inflated number of changes associated with post-gap acquisition dates. In these cases, users may choose to remove

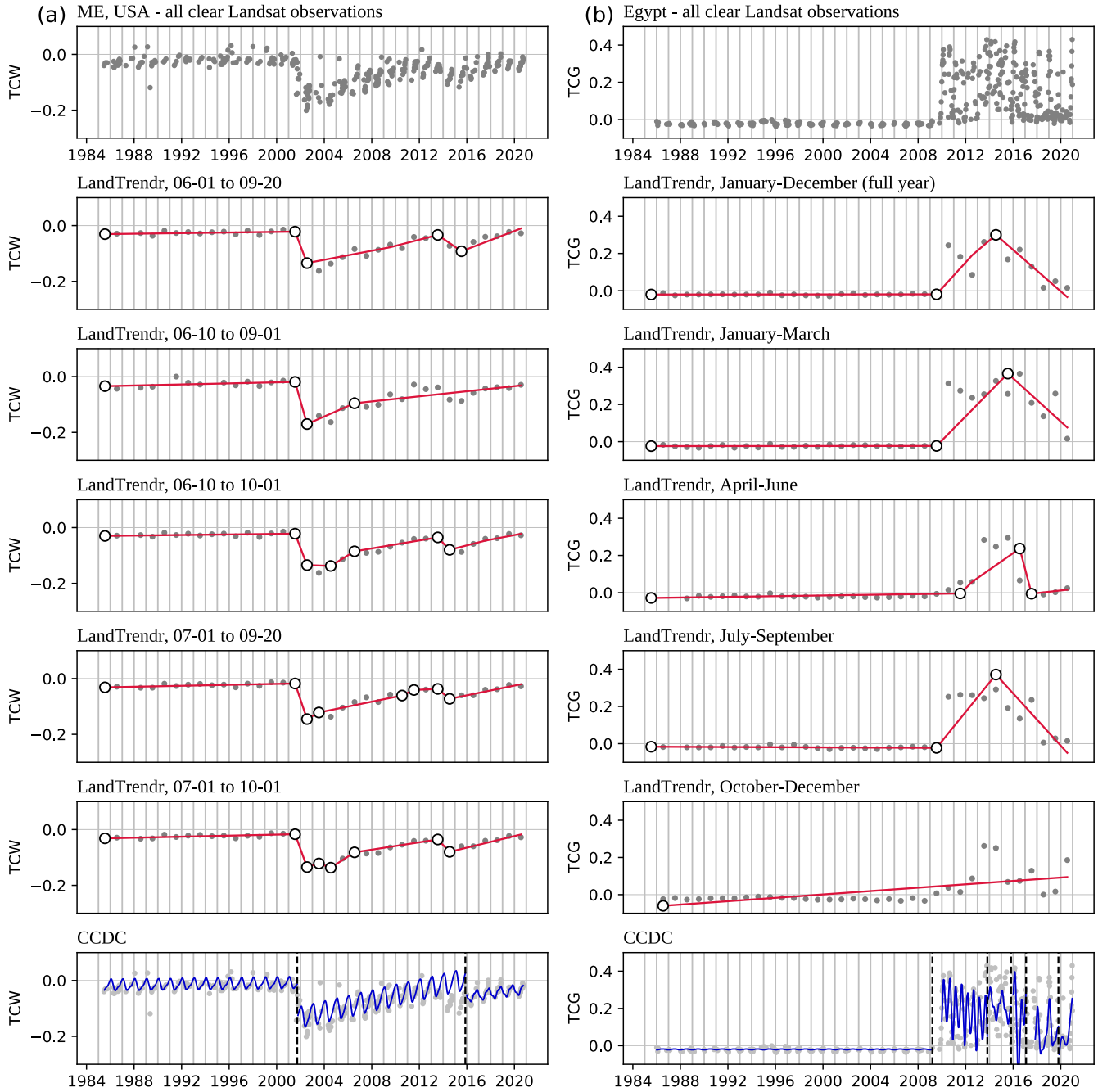

Fig. 3. Comparison of LandTrendr trajectories for different compositing periods and CCDC segmentation results for (a) forest disturbance in Maine, USA (45.4189°, −69.8050°), and (b) agricultural expansion as part of the Sharq El Owainat project, south-western Egypt (22.7799°, 28.5386°). Results are visualized using Tasseled Cap Wetness (TCW) for (a) and Tasseled Cap Greenness (TCG) for (b). Both algorithms are relatively consistent in identifying the timing of the initial change in cover for both sites, with the exception of the October-December period for the Egypt example, where no breaks are identified. Note how the number and placement of subsequent LandTrendr vertices varies depending on the compositing period while only a single result is obtained for CCDC since the CCDC approach uses all available observations and does not require users to specify a compositing period.

Table 3
Examples of studies using CCDC and CCDC-like temporal segmentation, including process of interest, study area, use of the temporal domain, and spectral inputs used for break detection.

Study	Process	Study area	Temporal period	Spectral inputs*
Zhu and Woodcock, 2014	Land cover change	Coastal New England, United States	All available imagery < 80% cloud cover, 1982–2011	Blue, Green, Red, NIR, SWIR1, SWIR2, Brightness Temperature
Fu and Weng, 2016	Land use/land cover change, urbanization	Atlanta metropolitan area, Georgia, United States	All available imagery < 90% cloud cover, 1984–2011	Surface reflectance, Brightness Temperature, NDVI
Sulla-Menashe et al., 2016**	Forest response to climate change	Boreal forests east of Canadian Rockies	All available imagery, 1984–2011	Not specified
Awty-Carroll et al., 2019a	Mangrove dynamics	The Sundarbans, Bangladesh/ India	All available imagery, January 1988 to June 2018	Green, Red, NIR, SWIR1, SWIR2
Shimizu et al., 2019a**	Changes in tropical forest (S1 fusion)	Bago region, Central Myanmar	All Landsat 8 imagery < 70% cloud cover and Sentinel-1 imagery in IW mode (ascending and descending), 2014–2018	TCB, TCG, TCW, TCA, NBR (L8); VV, VH (S1)
X. Tang et al., 2019	Near-real-time change detection (NRT-CCDC)	Amazon Basin, Pará and Rondônia in Brazil and Southern Colombia	Daily 250 m NDVI data, view zenith angle < 35 degrees, 2013–2015	NDVI
Brown et al., 2019	Land cover classification and change (LCMAP)	Select sites across conterminous United State	USGS Analysis Ready Data (ARD), 1985–2017	Green, Red, NIR, SWIR1, SWIR2
Arévalo et al., 2020b	Land change and post-disturbance recovery	Colombian Amazon	All available imagery < 80% cloud cover, 1997–2016	Blue, Green, Red, NIR, SWIR1, SWIR2
Berhane et al., 2020	Land use/land cover change	Midwestern United States	All available imagery < 80% cloud cover, 1982–2017	Blue, Red, Green, NIR, SWIR1, SWIR2, Brightness Temperature
Bullock et al., 2020a	Land cover and condition change	Selected sites across conterminous United States	All available imagery, 1984–2015	Blue, Green, Red, NIR, SWIR1, SWIR2
Bullock et al., 2020b*	Deforestation and forest degradation	Rondônia, Western Brazil	All available imagery, 1990–2013	GV, NPV, Soil, and Shade endmembers; NDFI
Deng and Zhu, 2020	Subpixel changes in urban impervious surfaces	Broome County, New York, United States	All available imagery < 20% cloud cover, 2000–2014	Blue, Green, Red, NIR, SWIR1, SWIR2
Guan et al., 2020	Urbanization and improvements from BRDF correction	Tianjin, China	All available imagery < 80% cloud cover, 1985–2018	Blue, Green, Red, NIR, SWIR1, SWIR2, Brightness Temperature
Chen et al., 2021	Deforestation and forest degradation (CCDC-SMA)	Country of Georgia	All available imagery (original bands), day 150 to day 300 (endmembers), 1987–2019	Blue, Green, Red, NIR, SWIR1, SWIR2; GV, NPV, Soil, and Shade endmembers; NDFI
Yu et al., 2021	Urban vegetation dynamics	Shenzhen megacity, southern China	All available imagery, 2000–2020	EVI
Xu et al., 2021	Citrus planting dynamics	Xunwu County, Jiangxi Province, China	All available imagery, 1986–2018	Blue, Green, Red, NIR, SWIR1, SWIR2, NDVI, NBR, NDFI

* Spectral Index abbreviations: GV = Green Vegetation endmember, NDVI = Normalized Difference Vegetation Index, NDFI = Normalized Difference Fraction Index, NPV = Non-Photosynthetic Vegetation endmember, TCA = Tasseled Cap Angle, TCB = Tasseled Cap Brightness, TCG = Tasseled Cap Greenness, TCW = Tasseled Cap Wetness.
** Use simplified CCDC-like harmonic modeling approaches.

years with sparse acquisition records from analysis (e.g., Arévalo et al., 2020b). Similarly, increases in the frequency of observations results in a shorter period of time needed to flag a change. For example, Brown et al., (2019) found that when running CCDC on Landsat Analysis Ready Data (Dwyer et al., 2018; Egorov et al., 2019), change detection rates increased in orbital path overlap (sidelap) zones and during periods when multiple satellites are in operation, such as from April 1999 to November 2011 when Landsats 5 and 7 were both in operation. These effects were mitigated by dynamically adjusting the number of observations needed to detect a change; however, this custom modification has not been incorporated into all versions of CCDC and is not currently available in the Earth Engine implementation. Thus, Earth Engine users working with merged Landsat collections across larger study areas spanning multiple scenes should consider spatial and temporal inconsistencies and may want to apply additional filters on path overlaps and row endlaps or run separate models for individual scene-based image stacks. Changes in observation density and irregularity also affect the use of harmonic regression models for time series reconstruction (i.e., generating synthetic images), and a data density of at least seven observations per year is recommended for Landsat time series analysis (Zhang et al., 2021).

Another important set of considerations for temporal segmentation are the time series start and end dates and length of time series being segmented. LandTrendr is considered an "offline" approach in that the full series of composited values is used to determine the optimal set of segments and vertices (Zhu, 2017). The user must specify the maximum number of segments to use in model fitting, and changing the time series start and end dates can affect the trajectory fitting and timing of vertices (Fig. 4). Changing the number of segments used for fitting can also result in differences in fitted trajectories, and it is generally advisable to increase the number of allowable segments in studies of frequently disturbed landscapes. Number of segments should also generally be increased relative to the length of time series records to account for increasing likelihood of multiple disturbance events occurring over longer time periods.

Unlike LandTrendr, CCDC employs an "online" approach to segmentation such that observations are considered in an iterative, forward-looking manner when determining the placement of breaks (Zhu, 2017). As a result, CCDC models are sensitive to values at the beginning of fitting periods, and stability tests are included in the fitting procedure to encourage more stable model initialization (Zhu et al., 2020). Changing the start year of input time series can significantly influence the timing of breaks as well as the fit of harmonic segments, especially if monitoring begins during a relatively unstable period (e.g., Fig. 4). CCDC segmentation results may also change as new dates of imagery are added to update time series and results, with longer CCDC segments based on greater numbers of observations and strong temporal signatures tending to be more robust to the addition of new observations.

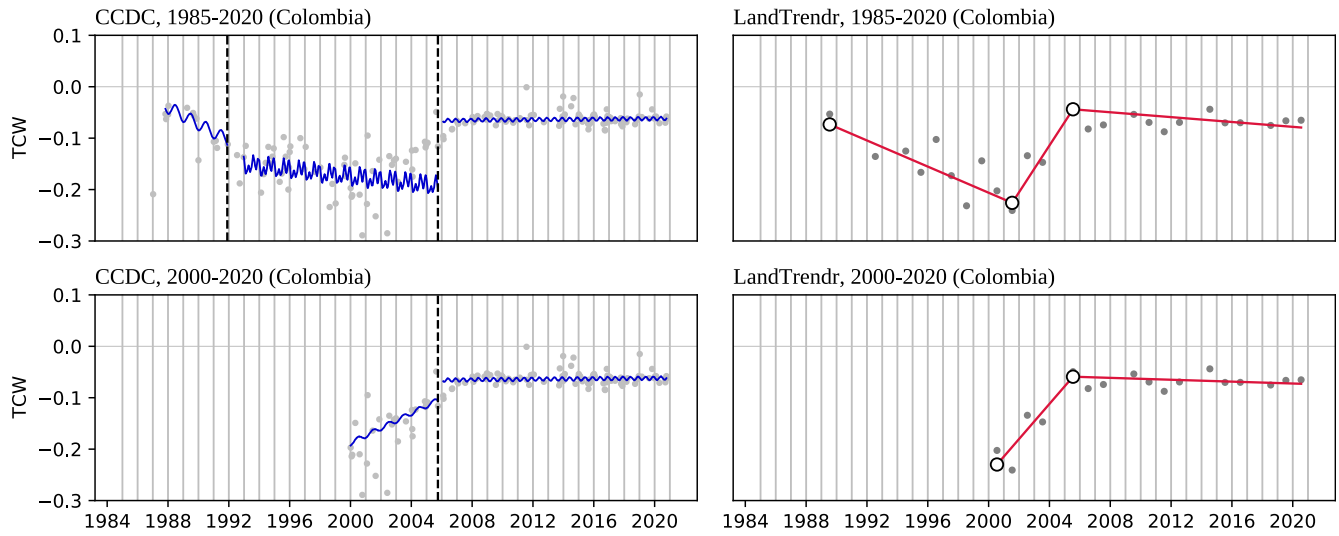

Fig. 4. Segmentation results for different periods for an example of forest regeneration in Colombia (1.3808°, −71.8826°). Changing the start year resulted in fewer segments and although all models identified a change around 2005, the slope and amplitude of the preceding CCDC segment (2000–2005) differed from the comparable time period for the 1985–2020 model. The LandTrendr segments also show slight differences in their rates of change.

2.3. Use of the spectral domain

Another fundamental consideration when performing temporal segmentation is the choice of spectral inputs. When applied to Landsat time series, typical inputs include surface reflectance and brightness temperature measurements (i.e., Landsat bands) and multi-spectral indices and transforms, though time series from other sensors and of other continuous values such as classification probabilities or climatic variables can also be used.

LandTrendr was designed as a univariate model, where only one band, index, or feature is used in segmentation. It is important that users select an input that best captures the change process of interest (see Table 2 for examples**)**. The original LandTrendr implementation (Kennedy et al., 2010) was tested using the Normalized Burn Ratio (NBR),

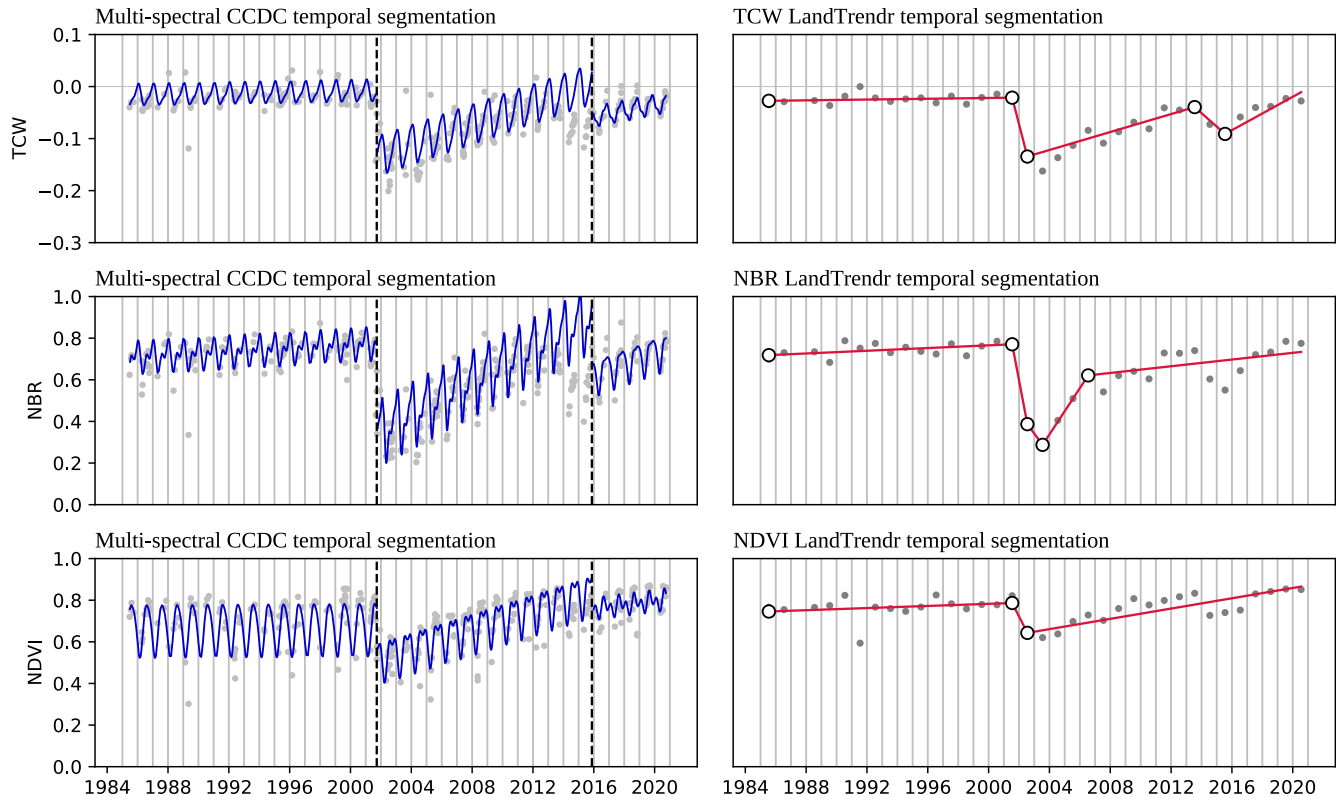

Fig. 5. CCDC and LandTrendr temporal segmentation results for the Normalized Burn Ratio (NBR), the Normalized Difference Vegetation Index (NDVI), and Tasseled Cap Wetness (TCW) for the same Maine, USA, site shown in Fig. 1 (45.4189°, −69.8050°). CCDC models were fit in a multi-spectral context, resulting in break information that is shared across input features/bands, as illustrated by the consistent number of segments and locations of breaks in CCDC results. In contrast, the LandTrendr algorithm is univariate, with segmentation performed on a single band, index, or other continuous value, resulting in different numbers of segments and placement of vertices, depending on the input.

Tasseled Cap Wetness (TCW), and the Normalized Difference Vegetation Index (NDVI), and these indices remain common choices (Table 2). Comparisons by Cohen et al. (2020) and Cohen et al. (2018) suggest that SWIR-based features tend to exhibit the strongest performance for forest disturbance detection in a univariate context, with TCW having the lowest overall error rates. Given the sensitivity of NDVI to vegetation cover, NDVI time series have also been employed in studies using LandTrendr to characterize mining disturbances (Xiao et al., 2020; Yang et al., 2018), cropland conversion (Zhu et al., 2019) and more general land cover change (Rathnayake et al., 2020); however, NDVI is known to be sensitive to soil background and atmospheric effects as well. Time series of Tasseled Cap Angle (TCA), which characterizes percent vegetation cover based on the arctangent of the TCG-TCB ratio, can be a useful transform when incorporating Landsat MSS data into the time series record, as the MSS sensor does not include SWIR bands (Pflugmacher et al., 2012). LandTrendr has also been effectively applied to annual time series of other continuous biophysical variables such as biomass time series (Main-Knorn et al., 2013) and cropland and agricultural land classification probabilities (Dara et al., 2018; Yin et al., 2018).

Assuming a univariate relationship between the change processes of interest and the time series of observed values simplifies interpretation of the results of the segmentation process, and vertices can be applied to other bands/indices such that the timing of changes remains consistent across multiple input features. Extending segmentation results to other bands also enables generation of smoothed values that can be used for multispectral classification. However, different inputs may produce different trajectories (Fig. 5), and leveraging relationships between these results requires additional post-processing, such as secondary classification or "stacking" methods (Cohen et al., 2020, 2018; Healey et al., 2018).

While CCDC can be configured for single-band change detection (e.g., Yu et al., 2021), CCDC segmentation is typically performed using multiple spectral bands or indices and univariate tests for each band are combined in order to identify breaks. By considering change in a multispectral context, CCDC is less sensitive to individual inputs and break detection is consistent across inputs and derived indices (Fig. 5). In most cases, CCDC is run on surface reflectance inputs with the Blue band (4.5–5.2 nm) omitted due to strong atmospheric influence (Table 3). CCDC has also been run on derived indices, such as the Normalized Difference Fraction Index (NDFI), which uses an endmember-based unmixing approach to provide enhanced information on fractional cover (Bullock et al., 2020b; Chen et al., 2021), and has been applied to time series from other sensors, such as dual-polarized radar inputs from Sentinel-1 (Shimizu et al., 2019a) and MODIS NDVI (X. Tang et al., 2019). However, when multiple inputs contribute to the change detection process, interpretation of CCDC segmentation results can be less straightforward than those from univariate LandTrendr models. Furthermore, while including harmonic terms at several frequencies and employing a regularization approach enables flexibility and generalization in model fitting, it is important to consider whether temporal patterns in the observation record are well-represented using CCDC's inherently cyclic model formulation. For example, Cohen et al. (2020) found that COLD, which uses a very similar modeling and break detection approach as CCDC, tended to show a greater reliance on NIR-based indices than LandTrendr for forest disturbance detection, potentially due to improved characterization of forest phenology from all available observations using harmonic models.

2.4. Additional model parameterization

In addition to spectral and temporal attributes of time series inputs, LandTrendr and CCDC have a number of other tunable parameters (see Tables 4 and 5 for default parameter values for Earth Engine and other key reference implementations). Although both algorithms are generally robust to small parameterization changes, different combinations of parameters can produce different segmentation results and parameter values are often selected using example sites prior to scaling to a full study area. For example, in developing a monitoring system to characterize changes in biomass in the Pacific Northwest, Kennedy et al. (2018a) developed three LandTrendr parameterizations for SWIR1, TCW, and NBR, with best model proportion and p-value parameters increased when using SWIR1 and fewer segments used for TCW. When working with CCDC, the number of observations required to flag a change and the chi-square probability threshold for change detection are perhaps the most critical parameters to be tuned. For example, Brown et al. (2019) dynamically adjusted the consecutive observations parameter based on frequency of time series inputs, whereas Cohen et al. (2020) decreased the chi-square probability from 0.99 to 0.90 to better tolerate commission errors.

Other studies have included more formal sensitivity analyses to optimize segmentation results. For example, Xu et al. (2019) used a parametric tuning approach to systematically select a set of optimal parameters for LandTrendr segmentation and post-processing, and found the greatest variability in values for spikeThreshold, vertexCountOvershoot, recoveryThreshold, and bestModelProportion across different spectral inputs, specifically NBR, NDVI, NDMI, the Red band, and the SWIR1 band. In the CCDC context, Awty-Carroll et al. (2019b) used a manual interpretation of model results to select a value for the lambda parameter and found that a value of 1 (rather than the default of 20) worked best for their use case.

Unless otherwise noted, the examples presented in this paper were generated using the Earth Engine default parameters, with two notable exceptions. First, the LandTrendr default best model proportion was decreased from 1.25 (Table 4) to 0.75, as the former typically produced very poor results and the latter is more consistent with most published case studies. Second, because we worked with scaled surface reflectance values that were divided by 10000, we also re-scaled our CCDC lambda parameter from 20 (Table 5) to 0.002.

2.5. Outputs and data products

Whereas visualizing segmentation results for individual pixels is essential for understanding spectral-temporal relationships and parameterizing algorithms to detect change processes of interest, development of spatial products is typically the goal for most temporal segmentation analyses. The LandTrendr and CCDC temporal segmentation functions available in Google Earth Engine and from other sources (Table 1) operate on a per-pixel basis and typically generate outputs in the form of array images. Unlike conventional rasters that store only one value or observation per band, array images can contain multi-dimensional arrays of values for each pixel, enabling more complex indexing of the spectral-temporal domain. This format lends itself well to temporal segmentation where multi-spectral segment and vertex/break information must be stored for each pixel. For example, CCDC stores the following information per pixel: (a) segment start and end dates and dates of detected breaks, (b) number of observations per segment, (c) change probability per detected change, (d) CCDC coefficients corresponding to intercept, slope and pairs of harmonic sine and cosine terms by number of temporal segments, (e) Root Mean Square Error (RMSE) of each temporal segment for each input spectral band, and (f) magnitude of change for each input band. Similarly, the output from the LandTrendr algorithm consists of: (a) the year of observations, (b) the source value of observations, (c) the source value of observations fitted to segment lines between vertices (Fit-To-Vertex, or FTV), (d) a Boolean indicator for whether an observation is considered a segmentation vertex, (e) the RMSE of the FTV values, relative to the source values, and (f) complete time series FTV values for additional bands in the collection greater than band 1.

To summarize information and generate more standard map products, array images are subset or "sliced" in the temporal domain to extract segment, vertex, and break attributes that can be sorted and

Table 4
LandTrendr parameters for reference implementations.

Input*	Type	Earth Engine default	Kennedy et al. (2010)	Kennedy et al. (2018a,b)
timeSeries	ImageCollection	user-specified	NBR, NDVI, TCW	NBR
maxSegments	Integer	user-specified	4, 5, 6	6
spikeThreshold ("desawtooth val")	Float	0.9	1.0, 0.9, 0.75	0.9
vertexCountOvershoot	Integer	3	0, 3	3
preventOneYearRecovery	Boolean	false	n/a	n/a
recoveryThreshold	Float	0.25	1, 0.5, 0 25	0.25
pvalThreshold	Float	0.1	0.05, 0.1, 0.2	0.05
bestModelProportion	Float	1.25	n/a	0.75
minObservationsNeeded ("minneeded")	Integer	6	n/a	6

*See Kennedy et al. (2010) and https://developers.google.com/earth-engine/apidocs/ee-algorithms-temporalsegmentation-landtrendr for parameter descriptions.

Table 5
CCDC parameters for reference implementations.

Input*	Type	Earth Engine default	CCDC Version 12.3
collection	ImageCollection	user-specified	user-specified
breakpointBands	List	null (if unspecified, all bands are used)	Green, Red, NIR, SWIR1, SWIR2
tmaskBands	List	null (if unspecified, Tmask not used)	Green, SWIR1
minObservations	Integer	6	6
chiSquareProbability	Float	0.99	0.99
minNumOfYearsScaler	Float	1.33	1
dateFormat	Integer	0 (jDays)	Julian date
lambda	Float	20	20
maxIterations	Integer	25,000	1000

* See https://developers.google.com/earth-engine/apidocs/ee-algorithms-temporalsegmentation-ccdc for parameter descriptions.

combined in a variety of ways. Although variable-length CCDC arrays are inherently more complex than LandTrendr arrays, which are structured in terms of number of years, both can be used to produce very similar products (Table 6). For example, both algorithms can be used to map the time of first, last and/or largest change over a specified time horizon and provide information on the magnitude of change between two segments (Fig. 6). Both also provide RMSE as a metric of model fit, and segmentation results can be used to generate "synthetic" or fitted spectral values that are essentially smoothed in the temporal domain. These synthetic images can be used in place of observed imagery or composites for change detection and/or land cover classification (e.g., Healey et al., 2018; Kennedy et al., 2018a). CCDC segmentation outputs

Table 6
Examples of map products that can be generated from the outputs of LandTrendr and CCDC segmentation.

Product category	LandTrendr products	CCDC products
Timing and frequency of change	Year of detection (first, last, largest); number of changes	Date of change (first, last, largest); number of changes
Magnitude	Magnitude of spectral change calculated as the spectral distance between vertices	Magnitude of spectral change calculated as the spectral difference between end and start points of adjacent segments
Model fit assessment	RMSE of fitted temporal segment (composite observations to fitted values)	RMSE of fitted temporal segments (all observations to fitted values)
Predicted image	Fitted values at an annual time step; fit-to-vertex result includes multi-band output	Synthetic image predicted for a specific date from segment coefficients
Additional segment attributes	Duration, rate of spectral change, pre-change value, Change Signal-to-Noise Ratio (CSNR, previously DNSR)	Intercept, slope, sine/cosine coefficients

a set of regression coefficients that can also be used for classification of segments and/or specific time periods (e.g., Brown et al., 2019; Pasquarella et al., 2018; Xian et al., 2021). Additional attributes that can be derived from LandTrendr segmentation results include segment duration and rate of change, pre-change FTV, and a Change Signal-to-Noise Ratio (CSNR), previously referred to as the Disturbance Signal-to-Noise Ratio (DNSR), which is calculated by dividing the change signal by the plot-level noise estimated by the model RMSE (Cohen et al., 2018).

2.6. Tools and visualization

The availability of LandTrendr and CCDC functions in Google Earth Engine has enabled the development of new tools that facilitate running these algorithms and interacting with their outputs. Graphical user interfaces for plotting time series and LandTrendr fitted data and mapping disturbances and visualizing change are available in the UI Applications section of the LT-GEE Guide (emapr.github.io/LT-GEE/). Current tools include Pixel Time Series Plotter, Change Mapper, Fitted Index Delta RGB Mapper, and Time Series Animator interfaces, as well as example scripts for producing maps of vegetation distance, gain, and loss. Similarly, a set of new interactive tools to run and visualize time series of CCDC fitted results, create maps of CCDC coefficients (including transforms such as phase and amplitude) and predicted images, and create land cover and change maps are described in Arévalo et al. (2020a). Both sets of tools also offer their own application programming interface (API) functionality that allows users more flexibility to interact with the algorithm outputs.

To facilitate comparisons like those shown in this study, we have also developed a tool to visualize and compare segmentation results from LandTrendr and CCDC (see Supplemental materials). This tool runs both algorithms on Landsat time series for the same pixel, allowing users to interactively adjust inputs and parameters and view segmentation results. As implementations of CCDC, LandTrendr, and other temporal segmentation algorithms continue to mature, visualization and other pre- and post-processing toolkits will be essential for facilitating adoption by broader remote sensing and applications communities and building a deeper understanding of best practices in terms of use cases and parameterization choices.

3. Discussion and conclusions

When selecting among a growing suite of temporal segmentation algorithms, users must consider the variety and complexity of land cover change processes of interest, including their temporal duration and expected spectral-temporal trajectories. Though LandTrendr and CCDC are both designed to automate extraction of reflectance characteristics and change event information from time series of satellite imagery, these methods are distinct in their use of the spectral and temporal domains, fitting approaches, and attributes of segmentation results. Both algorithms assume that a sequence of linear models can be used to identify and quantify periods of stability and change in surface properties, and both rely on the availability of sufficient high-quality measurements to

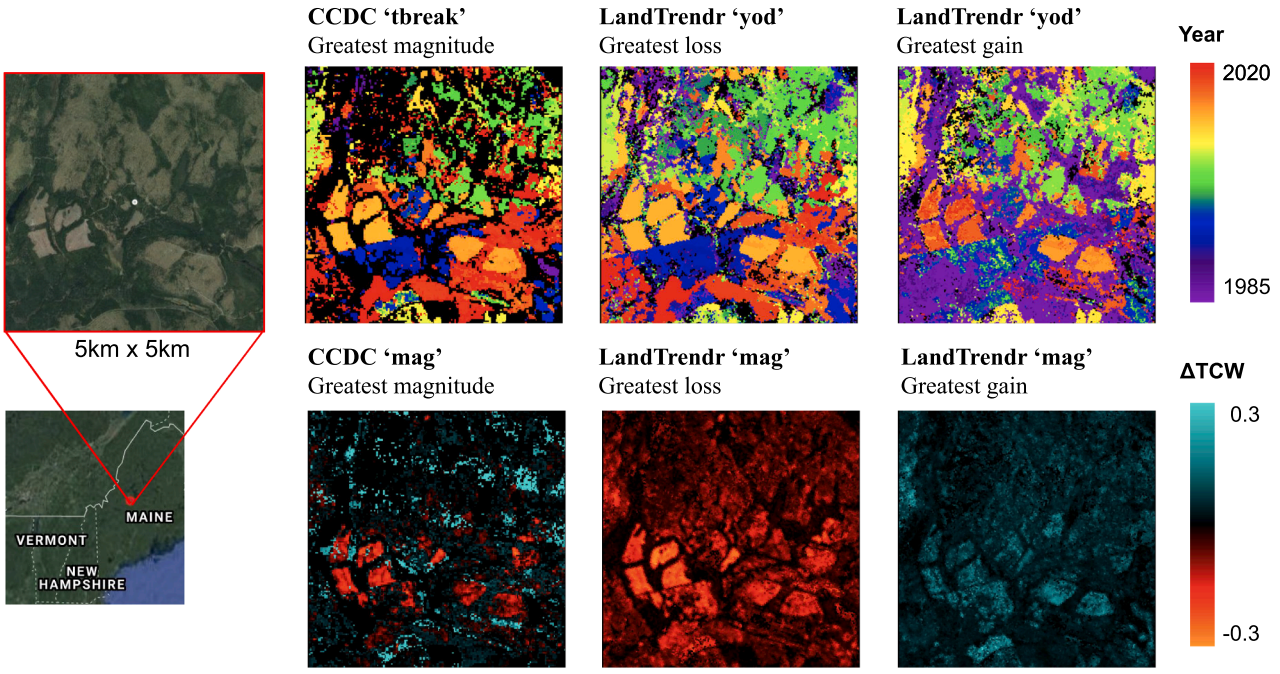

Fig. 6. Examples of LandTrendr and CCDC map products for a 5 km × 5 km site in Maine, USA. Top row shows results in terms of year of greatest change, with CCDC timing of break ('tbreak') maps including both positive and negative changes, whereas LandTrendr year of detection ('yod') results are separated in terms of greatest loss and greatest gain. Bottom row shows the associated magnitude of change ('mag') results in Tasseled Cap Wetness (TCW), and a high-resolution reference image is shown at left with a white point at the center of the image to indicate the example pixel used in Figs. 1, 3, and 5.

characterize patterns and processes of interest. LandTrendr typically uses univariate time series reduced to an annual time step to generate continuous reflectance trajectories, whereas CCDC uses all clear observations across multiple spectral bands or indices to perform break detection and characterize seasonal variability within segments. A summary of key comparisons is provided in Table 7.

Some important considerations for potential users can be broadly described in terms of scalability, sensitivity, reproducibility, and accuracy of algorithms and outputs. Although both the LandTrendr and CCDC algorithms can now be run in Google Earth Engine, users still face notable trade-offs balancing the precision of information generated by the segmentation process and associated storage and runtime. LandTrendr is less computationally intensive than CCDC and can be applied over large areas with relative ease. CCDC is arguably less scalable because of larger computing and storage requirements, and generating CCDC results at national and continental scales may remain prohibitive for most users. However, CCDC segmentation results include information on seasonal dynamics as well as more precision in estimating the timing of disturbances and other land cover changes that may be critical for some mapping and monitoring applications. For example, LandTrendr is well suited to providing yearly disturbance estimates, but if sub-yearly information is critical, then CCDC is likely a better choice, assuming a sufficient number of high quality observations are available for the time period(s) of interest.

Users should also consider the sensitivity of the LandTrendr and CCDC algorithms with regard to inputs and parameters. LandTrendr users must make informed choices regarding compositing period and individual spectral indices used for segmentation, and small changes in spectral inputs and key parameters can substantially impact segmentation results. To optimize fitting for particular regions, ecosystems, and change processes, LandTrendr parameter testing is recommended to calibrate inputs and model settings. CCDC users may also adjust a number of model specifications, including input bands used for segmentation and regression tuning parameters, and an exploratory calibration phase is also highly recommended. As a multivariate model that uses all available observations, the CCDC approach is generally not as sensitive to inputs and small parameter changes as LandTrendr; however, CCDC's iterative fitting and change detection approach is more sensitive to initial conditions and changes in observation frequency.

Sensitivity of segmentation results to spectral and temporal inputs and parameterization choices also plays an important role in reproducibility. Because temporal segmentation is highly dependent on a number of user-specified decisions and a given result represents just one of potentially many possible outcomes, thorough documentation of algorithm inputs is essential for ensuring reproducibility of results. Users, particularly those working with Earth Engine implementations, are therefore encouraged to provide complete details on not only spectral and temporal properties of image inputs, but also parameter values and any post-processing decisions. As image archives continue to be updated with new acquisitions, there will also be unprecedented opportunities to revisit previous temporal segmentation studies and establish best practices for updating and improving results.

A final point of consideration involves the accuracies of disturbance maps generated from CCDC and LandTrendr. CCDC and LandTrendr fundamentally differ in their modeling approaches, and therefore users should expect to see differences in resulting land cover and change products. CCDC is well suited for detecting high-magnitude disturbances and land cover changes with minimal tuning across diverse land cover types. However, it has been found to be less suitable for detecting more gradual land cover transitions that are not associated with a distinct disturbance event, such as insect disturbances, partial/selective harvests, and vegetation regrowth (Cohen et al., 2017), though modifications to the core CCDC approach such as COLD (COntinuous monitoring of Land Disturbance) can improve detecting such transitions (Zhu et al., 2020). LandTrendr targets both discrete and gradual trends and can be fine-tuned to specific processes of interest. Multi-spectral ensembles that combine information from multiple LandTrendr runs can also be used to produce more robust change detection results (Cohen et al., 2018; De Marzo et al., 2021).

Continued maturation of temporal segmentation algorithms and

Table 7
Summary of key characteristics for LandTrendr and CCDC.

	LandTrendr	CCDC
Full name	Landsat-based detection of Trends in Disturbance and Recovery	Continuous Change Detection and Classification
Segmentation inputs	Annual observations or composites	All high-quality observations
Use of spectral domain	Univariate; segmentation based on one band or index	Multi-spectral; multiple input bands or indices considered in change detection
Model description	Linear regression-based vertex identification and selection used to model spectral-temporal trajectory	Harmonic regression used to model seasonality, trend, and breaks; Least Absolute Shrinkage and Selection Operator (LASSO) by default
Model structure	Continuous series of segments and vertices	Discontinuous series of segments and breaks
Monitoring approach	"Offline"; full time series is considered in identifying segments and vertices	"Online"; predictions are made in an iterative, forward-looking manner
Interpretation	Vertices indicate change in spectral trajectory; segments labeled as stable or changing	Breaks represent land cover or condition change; segments labeled in terms of land cover and/or trends
Visualization & assessment	LandTrendr UI Tools (emapr.github.io/LT-GEE/)	CCDC User Interface (UI) Tools (Arévalo et al., 2020a)
Smoothed/ synthetic imagery	Fit-to-vertex values along trajectory, annual time step	Predicted reflectance values for Julian date
Temporal constraints	Suggest at least one observation per year for best results, though years may be skipped. Observations selected for consistent phenology. Best suited for study areas with consistent near-anniversary-date imagery.	Requires at least 12 observations for basic 4-term harmonic model; suggest at least 3 observations per additional coefficient. Better suited for study areas/time periods with dense observation records.
Relative computational requirements	Less compute/memory-intensive	More compute/memory-intensive

their implementations has also resulted in opportunities to improve segmentation outputs by combining desirable features of each segmentation algorithm. For example, a version of the F-statistic test used by LandTrendr has been integrated as a post-processing step for CCDC results. In this "commission test," breaks that do not significantly improve model fit are eliminated from CCDC change results, resulting in improved land cover and land cover change products (Bullock et al., 2020a). Alternatively, harmonic features can be estimated using fixed window time series (e.g., Adams et al., 2020; Wilson et al., 2018), and associated regression coefficients may be used as inputs to or in conjunction with LandTrendr segmentation results to provide additional information on more complex phenological cycles. Combinations of output maps generated with different algorithms and/or parameterization can also be leveraged to improve the quality of change detection results, and map-to-map comparisons (e.g., Cohen et al., 2017) and other ensembling approaches (Cohen et al., 2020; Healey et al., 2018; Hislop et al., 2019) provide new insights into the relative strengths and weaknesses of segmentation approaches for specific applications. However, ensemble approaches inherently require greater computational resources and data storage, and more rigorous assessment of tradeoffs between gains in accuracy and model complexity and interpretability represents an important direction for future research.

With a growing number of temporal segmentation algorithms now implemented natively in Google Earth Engine and being made available by the Earth Engine user community (e.g., Hamunyela et al., 2020), there are new opportunities to test these algorithms individually and in combination for a diverse array of possible applications. By having centralized code repositories and tools paired with versioned image collections available in a cloud-computing environment like Google Earth Engine, the effectiveness of different algorithms for detecting different types of change processes occurring in different types of ecosystems/landscapes can be more formally tested and best practices for selecting and parameterizing different algorithms for specific types of mapping and monitoring can be developed. Furthermore, users will increasingly have a choice between running temporal segmentation and other image pre- and post-processing algorithms themselves or developing applications on top of existing results and other "analysis-ready" feature sets and products. As existing cloud-based datasets and analysis tools continue to mature and evolve and new datasets and tools become available, ongoing comparison of conceptual and methodological differences, such as the CCDC-LandTrendr comparison presented here, will be essential for both informed use and future development of image processing algorithms and their associated products.

Declaration of Competing Interest

The authors declare that they have no known competing financial interests or personal relationships that could have appeared to influence the work reported in this paper.

Acknowledgements

We gratefully acknowledge Justin Braaten, Curtis Woodcock, and our anonymous reviewers for their insightful comments and suggestions for improving this manuscript. We would also like to acknowledge Christopher Holden for early discussions that led to the comparisons presented here. VJP and KHB were supported in part by USGS/Landsat Science Team award #140G118C0006. PA and EB were funded through NASA research grant #80NSSC18K0994.

Appendix A. Supplementary material

Supplementary data to this article can be found online at https://doi.org/10.1016/j.jag.2022.102806.

References

Adams, B., Iverson, L., Matthews, S., Peters, M., Prasad, A., Hix, D.M., 2020. Mapping Forest Composition with Landsat Time Series: An Evaluation of Seasonal Composites and Harmonic Regression. Remote Sens. 12 (4), 610. https://doi.org/10.3390/rs12040610.

Arévalo, P., Bullock, E.L., Woodcock, C.E., Olofsson, P., 2020a. A Suite of Tools for Continuous Land Change Monitoring in Google Earth Engine. Front. Climate 2. https://doi.org/10.3389/fclim.2020.576740.

Arévalo, P., Olofsson, P., Woodcock, C.E., 2020b. Continuous monitoring of land change activities and post-disturbance dynamics from Landsat time series: A test methodology for REDD+ reporting. Remote Sens. Environ. 238, 111051. https://doi.org/10.1016/j.rse.2019.01.013.

Awty-Carroll, K., Bunting, P., Hardy, A., Bell, G., 2019a. Using Continuous Change Detection and Classification of Landsat Data to Investigate Long-Term Mangrove Dynamics in the Sundarbans Region. Remote Sens. 11 (23), 2833. https://doi.org/10.3390/rs11232833.

Awty-Carroll, K., Bunting, P., Hardy, A., Bell, G., 2019b. An Evaluation and Comparison of Four Dense Time Series Change Detection Methods Using Simulated Data. Remote Sens. 11 (23), 2779. https://doi.org/10.3390/rs11232779.

Banskota, A., Kayastha, N., Falkowski, M.J., Wulder, M.A., Froese, R.E., White, J.C., 2014. Forest Monitoring Using Landsat Time Series Data: A Review. Can. J. Remote Sens. 40 (5), 362–384.

Berhane, T., Lane, C., Mengistu, S., Christensen, J., Golden, H., Qiu, S., Zhu, Z., Wu, Q., 2020. Land-Cover Changes to Surface-Water Buffers in the Midwestern USA: 25 Years of Landsat Data Analyses (1993–2017). Remote Sens. (Basel) 12 (5), 754. https://doi.org/10.3390/rs12050754.

Bright, B.C., Hudak, A.T., Kennedy, R.E., Braaten, J.D., Henareh Khalyani, A., 2019. Examining post-fire vegetation recovery with Landsat time series analysis in three western North American forest types. Fire Ecol. 15, 1–14.

Brooks, E.B., Wynne, R.H., Thomas, V.A., Blinn, C.E., Coulston, J.W., 2014. On-the-Fly Massively Multitemporal Change Detection Using Statistical Quality Control Charts and Landsat Data. IEEE Trans. Geosci. Remote Sens. 52 (6), 3316–3332.

Brown, J.F., Tollerud, H.J., Barber, C.P., Zhou, Q., Rover, J., 2019. Lessons learned implementing an operational continuous United States national land change monitoring capability: The Land Change Monitoring, Assessment, and Project

(LCMAP) approach. Remote Sens. Environ. https://doi.org/10.1016/j.rse.2019.111356.
Bullock, E.L., Woodcock, C.E., Holden, C.E., 2020a. Improved change monitoring using an ensemble of time series algorithms. Remote Sens. Environ. 238, 111165. https://doi.org/10.1016/j.rse.2019.04.018.
Bullock, E.L., Woodcock, C.E., Olofsson, P., 2020b. Monitoring tropical forest degradation using spectral unmixing and Landsat time series analysis. Remote Sens. Environ. 238, 110968. https://doi.org/10.1016/j.rse.2018.11.011.
Chaves, M.E.D., Picoli, M.C.A., Sanches, I.D., 2020. Recent Applications of Landsat 8/OLI and Sentinel-2/MSI for Land Use and Land Cover Mapping: A Systematic Review. Remote Sens. 12 (18), 3062. https://doi.org/10.3390/rs12183062.
Chen, S., Woodcock, C.E., Bullock, E.L., Arévalo, P., Torchinava, P., Peng, S., Olofsson, P., 2021. Monitoring temperate forest degradation on Google Earth Engine using Landsat time series analysis. Remote Sens. Environ. 265, 112648. https://doi.org/10.1016/j.rse.2021.112648.
Cohen, W., Healey, S., Yang, Z., Stehman, S., Brewer, C., Brooks, E., Gorelick, N., Huang, C., Hughes, M., Kennedy, R., Loveland, T., Moisen, G., Schroeder, T., Vogelmann, J., Woodcock, C., Yang, L., Zhu, Z., 2017. How Similar Are Forest Disturbance Maps Derived from Different Landsat Time Series Algorithms? Forests 8 (4), 98. https://doi.org/10.3390/f8040098.
Cohen, W.B., Healey, S.P., Yang, Z., Zhu, Z., Gorelick, N., 2020. Diversity of Algorithm and Spectral Band Inputs Improves Landsat Monitoring of Forest Disturbance. Remote Sens. 12 (10), 1673. https://doi.org/10.3390/rs12101673.
Cohen, W.B., Yang, Z., Healey, S.P., Kennedy, R.E., Gorelick, N., 2018. A LandTrendr multispectral ensemble for forest disturbance detection. Remote Sens. Environ. 205, 131–140.
Coppin, P., Jonckheere, I., Nackaerts, K., Muys, B., Lambin, E., 2004. Review ArticleDigital change detection methods in ecosystem monitoring: a review. Int. J. Remote Sens. 25 (9), 1565–1596.
Dara, A., Baumann, M., Kuemmerle, T., Pflugmacher, D., Rabe, A., Griffiths, P., Hölzel, N., Kamp, J., Freitag, M., Hostert, P., 2018. Mapping the timing of cropland abandonment and recultivation in northern Kazakhstan using annual Landsat time series. Remote Sens. Environ. 213, 49–60.
de Jong, S.M., Shen, Y., de Vries, J., Bijnaar, G., van Maanen, B., Augustinus, P., Verweij, P., 2021. Mapping mangrove dynamics and colonization patterns at the Suriname coast using historic satellite data and the LandTrendr algorithm. Int. J. Appl. Earth Obs. Geoinf. 97, 102293. https://doi.org/10.1016/j.jag.2020.102293.
De Marzo, T., Pflugmacher, D., Baumann, M., Lambin, E.F., Gasparri, I., Kuemmerle, T., 2021. Characterizing forest disturbances across the Argentine Dry Chaco based on Landsat time series. Int. J. Appl. Earth Obs. Geoinf. 98, 102310. https://doi.org/10.1016/j.jag.2021.102310.
Deng, C., Zhu, Z., 2020. Continuous subpixel monitoring of urban impervious surface using Landsat time series. Remote Sens. Environ. 238, 110929. https://doi.org/10.1016/j.rse.2018.10.011.
Dwyer, J.L., Roy, D.P., Sauer, B., Jenkerson, C.B., Zhang, H.K., Lymburner, L., 2018. Analysis Ready Data: Enabling Analysis of the Landsat Archive. Remote Sens. 10, 1363.
Egorov, A., Roy, D., Zhang, H., Li, Z., Yan, L., Huang, H., 2019. Landsat 4, 5 and 7 (1982 to 2017) Analysis Ready Data (ARD) Observation Coverage over the Conterminous United States and Implications for Terrestrial Monitoring. Remote Sens. 11 (4), 447. https://doi.org/10.3390/rs11040447.
Frazier, R.J., Coops, N.C., Wulder, M.A., 2015. Boreal Shield forest disturbance and recovery trends using Landsat time series. Remote Sens. Environ. 170, 317–327.
Frazier, R.J., Coops, N.C., Wulder, M.A., Kennedy, R., 2014. Characterization of aboveground biomass in an unmanaged boreal forest using Landsat temporal segmentation metrics. ISPRS J. Photogramm. Remote Sens. 92, 137–146.
Fu, P., Weng, Q., 2016. A time series analysis of urbanization induced land use and land cover change and its impact on land surface temperature with Landsat imagery. Remote Sens. Environ. 175, 205–214.
Gelabert, P.J., Rodrigues, M., de la Riva, J., Ameztegui, A., Sebastià, M.T., Vega-Garcia, C., 2021. LandTrendr smoothed spectral profiles enhance woody encroachment monitoring. Remote Sens. Environ. 262, 112521. https://doi.org/10.1016/j.rse.2021.112521.
Gómez, C., White, J.C., Wulder, M.A., 2016. Optical remotely sensed time series data for land cover classification: A review. ISPRS J. Photogramm. Remote Sens. 116, 55–72.
Gorelick, N., Hancher, M., Dixon, M., Ilyushchenko, S., Thau, D., Moore, R., 2017. Google Earth Engine: Planetary-scale geospatial analysis for everyone. Remote Sens. Environ. 202, 18–27.
Griffiths, P., Kuemmerle, T., Kennedy, R.E., Abrudan, I.V., Knorn, J., Hostert, P., 2012. Using annual time-series of Landsat images to assess the effects of forest restitution in post-socialist Romania. Remote Sens. Environ. 118, 199–214.
Grogan, K., Pflugmacher, D., Hostert, P., Kennedy, R., Fensholt, R., 2015. Cross-border forest disturbance and the role of natural rubber in mainland Southeast Asia using annual Landsat time series. Remote Sens. Environ. 169, 438–453.
Guan, Y., Zhou, Y., He, B., Liu, X., Zhang, H., Feng, S., 2020. Improving land cover change detection and classification with BRDF correction and spatial feature extraction using Landsat time series: a case of urbanization in Tianjin, China. IEEE J. Select. Top. Appl. Earth Observ. Remote Sens. 13, 4166–4177.
Hamunyela, E., Rosca, S., Mirt, A., Engle, E., Herold, M., Gieseke, F., Verbesselt, J., 2020. Implementation of BFASTmonitor Algorithm on Google Earth Engine to Support Large-Area and Sub-Annual Change Monitoring Using Earth Observation Data. Remote Sens. 12 (18), 2953. https://doi.org/10.3390/rs12182953.
Healey, S.P., Cohen, W.B., Yang, Z., Brewer, C.K., Brooks, E.B., Gorelick, N., Hernandez, A.J., Huang, C., Joseph Hughes, M., Kennedy, R.E., Loveland, T.R., Moisen, G.G., Schroeder, T.A., Stehman, S.V., Vogelmann, J.E., Woodcock, C.E., Yang, L., Zhu, Z., 2018. Mapping forest change using stacked generalization: An ensemble approach. Remote Sens. Environ. 204, 717–728.
Hemati, M., Hasanlou, M., Mahdianpari, M., Mohammadimanesh, F., 2021. A Systematic Review of Landsat Data for Change Detection Applications: 50 Years of Monitoring the Earth. Remote Sens. 13 (15), 2869. https://doi.org/10.3390/rs13152869.
Hislop, S., Jones, S., Soto-Berelov, M., Skidmore, A., Haywood, A., Nguyen, T.H., 2019. A fusion approach to forest disturbance mapping using time series ensemble techniques. Remote Sens. Environ. 221, 188–197.
Hossain, M.D., Chen, D., 2019. Segmentation for Object-Based Image Analysis (OBIA): A review of algorithms and challenges from remote sensing perspective. ISPRS J. Photogramm. Remote Sens. 150, 115–134.
Huang, C., Goward, S.N., Masek, J.G., Thomas, N., Zhu, Z., Vogelmann, J.E., 2010. An automated approach for reconstructing recent forest disturbance history using dense Landsat time series stacks. Remote Sens. Environ. 114 (1), 183–198.
Hughes, M., Kaylor, S., Hayes, D., 2017. Patch-Based Forest Change Detection from Landsat Time Series. Forests 8 (5), 166. https://doi.org/10.3390/f8050166.
Kennedy, R.E., Andréfouët, S., Cohen, W.B., Gómez, C., Griffiths, P., Hais, M., Healey, S.P., Helmer, E.H., Hostert, P., Lyons, M.B., Meigs, G.W., Pflugmacher, D., Phinn, S.R., Powell, S.L., Scarth, P., Sen, S., Schroeder, T.A., Schneider, A., Sonnenschein, R., Vogelmann, J.E., Wulder, M.A., Zhu, Z., 2014. Bringing an ecological view of change to Landsat-based remote sensing. Front. Ecol. Environ. 12 (6), 339–346.
Kennedy, R.E., Ohmann, J., Gregory, M., Roberts, H., Yang, Z., Bell, D.M., Kane, V., Hughes, M.J., Cohen, W.B., Powell, S., Neeti, N., Larrue, T., Hooper, S., Kane, J., Miller, D.L., Perkins, J., Braaten, J., Seidl, R., 2018a. An empirical, integrated forest biomass monitoring system. Environ. Res. Lett. 13 (2), 025004. https://doi.org/10.1088/1748-9326/aa9d9e.
Kennedy, R.E., Yang, Z., Cohen, W.B., 2010. Detecting trends in forest disturbance and recovery using yearly Landsat time series: 1. LandTrendr — Temporal segmentation algorithms. Remote Sens. Environ. 114 (12), 2897–2910.
Kennedy, R.E., Yang, Z., Cohen, W.B., Pfaff, E., Braaten, J., Nelson, P., 2012. Spatial and temporal patterns of forest disturbance and regrowth within the area of the Northwest Forest Plan. Remote Sens. Environ. 122, 117–133.
Kennedy, R., Yang, Z., Gorelick, N., Braaten, J., Cavalcante, L., Cohen, W., Healey, S., 2018b. Implementation of the LandTrendr Algorithm on Google Earth Engine. Remote Sens. 10 (5), 691. https://doi.org/10.3390/rs10050691.
Lister, A.J., Andersen, H., Frescino, T., Gatziolis, D., Healey, S., Heath, L.S., Liknes, G.C., McRoberts, R., Moisen, G.G., Nelson, M., Riemann, R., Schleeweis, K., Schroeder, T.A., Westfall, J., Wilson, B.T., 2020. Use of Remote Sensing Data to Improve the Efficiency of National Forest Inventories: A Case Study from the United States National Forest Inventory. Forests 11 (12), 1364. https://doi.org/10.3390/f11121364.
Main-Knorn, M., Cohen, W.B., Kennedy, R.E., Grodzki, W., Pflugmacher, D., Griffiths, P., Hostert, P., 2013. Monitoring coniferous forest biomass change using a Landsat trajectory-based approach. Remote Sens. Environ. 139, 277–290.
Meigs, G.W., Kennedy, R.E., Gray, A.N., Gregory, M.J., 2015. Spatiotemporal dynamics of recent mountain pine beetle and western spruce budworm outbreaks across the Pacific Northwest Region, USA. For. Ecol. Manage. 339, 71–86.
Mugiraneza, T., Nascetti, A., Ban, Y., 2020. Continuous Monitoring of Urban Land Cover Change Trajectories with Landsat Time Series and LandTrendr-Google Earth Engine Cloud Computing. Remote Sens. 12 (18), 2883. https://doi.org/10.3390/rs12182883.
Murillo-Sandoval, P.J., Gjerdseth, E., Correa-Ayram, C., Wrathall, D., Van Den Hoek, J., Dávalos, L.M., Kennedy, R., 2021. No peace for the forest: Rapid, widespread land changes in the Andes-Amazon region following the Colombian civil war. Glob. Environ. Change 69, 102283. https://doi.org/10.1016/j.gloenvcha.2021.102283.
Nguyen, T.H., Jones, S.D., Soto-Berelov, M., Haywood, A., Hislop, S., 2018. A spatial and temporal analysis of forest dynamics using Landsat time-series. Remote Sens. Environ. 217, 461–475.
Pasquarella, V.J., Holden, C.E., Kaufman, L., Woodcock, C.E., Nagendra, H., He, K., 2016. From imagery to ecology: leveraging time series of all available Landsat observations to map and monitor ecosystem state and dynamics. Remote Sens. Ecol. Conserv. 2 (3), 152–170.
Pasquarella, V.J., Holden, C.E., Woodcock, C.E., 2018. Improved mapping of forest type using spectral-temporal Landsat features. Remote Sens. Environ. 210, 193–207.
Pflugmacher, D., Cohen, W.B., Kennedy, E.R., 2012. Using Landsat-derived disturbance history (1972–2010) to predict current forest structure. Remote Sens. Environ. 122, 146–165.
Rathnayake, C.WM., Jones, S., Soto-Berelov, M., 2020. Mapping Land Cover Change over a 25-Year Period (1993–2018) in Sri Lanka Using Landsat Time-Series. Land 9 (1), 27. https://doi.org/10.3390/land9010027.
Reilly, M.J., Dunn, C.J., Meigs, G.W., Spies, T.A., Kennedy, R.E., Bailey, J.D., Briggs, K., 2017. Contemporary patterns of fire extent and severity in forests of the Pacific Northwest, USA (1985–2010). Ecosphere 8 (3), e01695. https://doi.org/10.1002/ecs2.1695.
Rodman, K.C., Andrus, R.A., Veblen, T.T., Hart, S.J., 2021. Disturbance detection in Landsat time series is influenced by tree mortality agent and severity, not by prior disturbance. Remote Sens. Environ. 254, 112244. https://doi.org/10.1016/j.rse.2020.112244.
Roy, D.P., Kovalskyy, V., Zhang, H.K., Vermote, E.F., Yan, L., Kumar, S.S., Egorov, A., 2016. Characterization of Landsat-7 to Landsat-8 reflective wavelength and normalized difference vegetation index continuity. Remote Sens. Environ. 185, 57–70.
Saxena, R., Watson, L.T., Wynne, R.H., Brooks, E.B., Thomas, V.A., Zhiqiang, Y., Kennedy, R.E., 2018. Towards a polyalgorithm for land use change detection. ISPRS J. Photogramm. Remote Sens. 144, 217–234.

Schneibel, A., Stellmes, M., Röder, A., Frantz, D., Kowalski, B., Haß, E., Hill, J., 2017. Assessment of spatio-temporal changes of smallholder cultivation patterns in the Angolan Miombo belt using segmentation of Landsat time series. Remote Sens. Environ. 195, 118–129.

Senf, C., Pflugmacher, D., Wulder, M.A., Hostert, P., 2015. Characterizing spectral–temporal patterns of defoliator and bark beetle disturbances using Landsat time series. Remote Sens. Environ. 170, 166–177.

Senf, C., Seidl, R., 2021. Mapping the forest disturbance regimes of Europe. Nat. Sustain. 4 (1), 63–70.

Shimizu, K., Ota, T., Mizoue, N., 2019a. Detecting Forest Changes Using Dense Landsat 8 and Sentinel-1 Time Series Data in Tropical Seasonal Forests. Remote Sens. 11 (16), 1899. https://doi.org/10.3390/rs11161899.

Shimizu, K., Ota, T., Mizoue, N., Yoshida, S., 2019b. A comprehensive evaluation of disturbance agent classification approaches: Strengths of ensemble classification, multiple indices, spatio-temporal variables, and direct prediction. ISPRS J. Photogramm. Remote Sens. 158, 99–112.

Sulla-Menashe, D., Friedl, M.A., Woodcock, C.E., 2016. Sources of bias and variability in long-term Landsat time series over Canadian boreal forests. Remote Sens. Environ. 177, 206–219.

Tang, D., Fan, H., Yang, K., Zhang, Y., 2019a. Mapping forest disturbance across the China-Laos border using annual Landsat time series. Int. J. Remote Sens. 40 (8), 2895–2915.

Tang, X., Bullock, E.L., Olofsson, P., Estel, S., Woodcock, C.E., 2019b. Near real-time monitoring of tropical forest disturbance: New algorithms and assessment framework. Remote Sens. Environ. 224, 202–218.

Tarrio, K., Friedl, M.A., Woodcock, C.E., Olofsson, P., Turlej, K., Zhu, Z., Loveland, T.R., Bullock, E., Arevalo, P.A., Holden, C., Pasquarella, V.J., Zhang, Y., 2019. Global Land Cover mapping and Estimation (GLanCE): a multitemporal Landsat-based data record of 21st century global land cover, land use and land cover change. ui.adsabs.harvard.edu, pp. GC21D–1317.

Vogeler, J., Slesak, R., Fekety, P., Falkowski, M., 2020. Characterizing over Four Decades of Forest Disturbance in Minnesota, USA. Forests 11 (3), 362. https://doi.org/10.3390/f11030362.

Vogelmann, J.E., Gallant, A.L., Shi, H., Zhu, Z., 2016. Perspectives on monitoring gradual change across the continuity of Landsat sensors using time-series data. Remote Sens. Environ. 185, 258–270.

Wilson, B.T., Knight, J.F., McRoberts, R.E., 2018. Harmonic regression of Landsat time series for modeling attributes from national forest inventory data. ISPRS J. Photogramm. Remote Sens. 137, 29–46.

Woodcock, C.E., Loveland, T.R., Herold, M., Bauer, M.E., 2020. Transitioning from change detection to monitoring with remote sensing: A paradigm shift. Remote Sens. Environ. 238, 111558. https://doi.org/10.1016/j.rse.2019.111558.

Wulder, M.A., Masek, J.G., Cohen, W.B., Loveland, T.R., Woodcock, C.E., 2012. Opening the archive: How free data has enabled the science and monitoring promise of Landsat. Remote Sens. Environ. 122, 2–10.

Wulder, M.A., White, J.C., Loveland, T.R., Woodcock, C.E., Belward, A.S., Cohen, W.B., Fosnight, E.A., Shaw, J., Masek, J.G., Roy, D.P., 2016. The global Landsat archive: Status, consolidation, and direction. Remote Sens. Environ. 185, 271–283.

Xian, G., Smith, K., Wellington, D., Horton, J., Zshou, Q., Li, C., Auch, R., Brown, J., Zhu, Z., Reker, R., 2021. Implementation of CCDC to produce the LCMAP Collection 1.0 annual land surface change product. Earth Syst. Sci. Data Discuss. 1–37.

Xiao, W.u., Deng, X., He, T., Chen, W., 2020. Mapping Annual Land Disturbance and Reclamation in a Surface Coal Mining Region Using Google Earth Engine and the LandTrendr Algorithm: A Case Study of the Shengli Coalfield in Inner Mongolia. China. Remote Sens. 12 (10), 1612. https://doi.org/10.3390/rs12101612.

Xu, H., Qi, S., Li, X., Gao, C., Wei, Y., Liu, C., 2021. Monitoring three-decade dynamics of citrus planting in Southeastern China using dense Landsat records. Int. J. Appl. Earth Obs. Geoinf. 103, 102518. https://doi.org/10.1016/j.jag.2021.102518.

Xu, H., Wei, Y., Liu, C., Li, X., Fang, H., 2019. A Scheme for the Long-Term Monitoring of Impervious−Relevant Land Disturbances Using High Frequency Landsat Archives and the Google Earth Engine. Remote Sens. 11 (16), 1891. https://doi.org/10.3390/rs11161891.

Yang, Y., Erskine, P.D., Lechner, A.M., Mulligan, D., Zhang, S., Wang, Z., 2018. Detecting the dynamics of vegetation disturbance and recovery in surface mining area via Landsat imagery and LandTrendr algorithm. J. Clean. Prod. 178, 353–362.

Ye, L.u., Liu, M., Liu, X., Zhu, L., 2021. Developing a new disturbance index for tracking gradual change of forest ecosystems in the hilly red soil region of southern China using dense Landsat time series. Ecol. Inform. 61, 101221. https://doi.org/10.1016/j.ecoinf.2021.101221.

Yin, H.e., Prishchepov, A.V., Kuemmerle, T., Bleyhl, B., Buchner, J., Radeloff, V.C., 2018. Mapping agricultural land abandonment from spatial and temporal segmentation of Landsat time series. Remote Sens. Environ. 210, 12–24.

Yu, W., Zhou, W., Dawa, Z., Wang, J., Qian, Y., Wang, W., 2021. Quantifying Urban Vegetation Dynamics from a Process Perspective Using Temporally Dense Landsat Imagery. Remote Sens. 13 (16), 3217. https://doi.org/10.3390/rs13163217.

Zhang, J., Shang, R., Rittenhouse, C., Witharana, C., Zhu, Z., 2021. Evaluating the impacts of models, data density and irregularity on reconstructing and forecasting dense Landsat time series, Egypt. J. Remote Sens. Space. Sci. 4, 100023. https://doi.org/10.1016/j.srs.2021.100023.

Zhu, L., Liu, X., Wu, L., Tang, Y., Meng, Y., 2019. Long-Term Monitoring of Cropland Change near Dongting Lake, China, Using the LandTrendr Algorithm with Landsat Imagery. Remote Sens. 11 (10), 1234. https://doi.org/10.3390/rs11101234.

Zhu, Z., 2017. Change detection using Landsat time series: A review of frequencies, preprocessing, algorithms, and applications. ISPRS J. Photogramm. Remote Sens. 130, 370–384.

Zhu, Z., Gallant, A.L., Woodcock, C.E., Pengra, B., Olofsson, P., Loveland, T.R., Jin, S., Dahal, D., Yang, L., Auch, R.F., 2016. Optimizing selection of training and auxiliary data for operational land cover classification for the LCMAP initiative. ISPRS J. Photogramm. Remote Sens. 122, 206–221.

Zhu, Z., Woodcock, C.E., 2014. Continuous change detection and classification of land cover using all available Landsat data. Remote Sens. Environ. 144, 152–171.

Zhu, Z., Woodcock, C.E., Olofsson, P., 2012. Continuous monitoring of forest disturbance using all available Landsat imagery. Remote Sens. Environ. 122, 75–91.

Zhu, Z., Zhang, J., Yang, Z., Aljaddani, A.H., Cohen, W.B., Qiu, S., Zhou, C., 2020. Continuous monitoring of land disturbance based on Landsat time series. Remote Sens. Environ. 238, 111116. https://doi.org/10.1016/j.rse.2019.03.009.